

Double Exchange model for nanoscopic clusters

D. Rotter¹, A. Valli¹, G. Sangiovanni^{1,2} and K. Held^{1a}

¹ Institute of Solid State Physics, Vienna University of Technology, 1040 Vienna, Austria

² Institute for Theoretical Physics and Astrophysics, University of Würzburg, Am Hubland, D-97074 Würzburg, Germany

Received: date / Revised version: date

Abstract. We solve the double exchange model on nanoscopic clusters exactly, and specifically consider a six-site benzene-like nanocluster. This simple model is an ideal testbed for studying magnetism in nanoclusters and for validating approximations such as the dynamical mean field theory (DMFT). Non-local correlations arise between neighboring localized spins due to the Hund's rule coupling, favoring a short-range magnetic order of ferro- or antiferromagnetic type. For a geometry with more neighboring sites or a sufficiently strong hybridization between leads and the nanocluster, these non-local correlations are less relevant, and DMFT can be applied reliably.

PACS. PACS-key describing text of that key – PACS-key describing text of that key

1 Introduction

In recent years, manganites such as $\text{La}_{1-x}\text{Ca}_x\text{MnO}_3$ (LCMO) have attracted great interest, mainly due to the colossal magnetoresistance [1]. In these materials, the crystal field splits the five 3d orbitals of the Manganese atoms into two e_g and three t_{2g} orbitals due to the perovskite structure. The latter are localized and as a consequence of Hund's exchange half-filled, forming a spin 3/2. This spin, the itinerant e_g electrons and their coupling, again by Hund's exchange, constitute the double exchange or ferromagnetic Kondo lattice model [2]. This arguably simplest model for manganites gives rise, in the bulk, to a ferromagnetic double exchange since a hopping energy of the e_g electrons can be gained only for a ferromagnetic (FM) alignment of the t_{2g} spins. For half-filled e_g bands one the other hand, the alignment of the t_{2g} spins is antiferromagnetic (AF) due to superexchange.

More recently, nanoclusters of manganites have been synthesized; and remarkably, a size-control of the charge and magnetic ordering in half-doped LCMO has been demonstrated [3,4]. Hence, size can be utilized to optimize the magnetic properties and the magnetoresistance of manganites for technological applications.

Not only these experiments, but also generally the emergence and peculiarity of magnetism in nan-

oclusters, motivates us to study the double exchange model:

$$H = -t \sum_{\langle ij \rangle \sigma} c_{i\sigma}^\dagger c_{j\sigma} - 2J \sum_i s_i S_i. \quad (1)$$

Here, $c_{i\sigma}^\dagger$ ($c_{i\sigma}$) are the creation (annihilation) operators of an electron at site i with spin σ , and t is the effective hopping amplitude corresponding to the double exchange process. S and s are the spins of the localized and mobile electrons respectively, J is the Hund's coupling between those spins. Henceforth we restrict ourselves to a Ising symmetry of the localized spins so that S_i simplifies to $S_i = \pm 1$, and $s_i = \frac{1}{2} \sum_{\sigma=\pm 1} c_{i\sigma}^\dagger \sigma c_{i\sigma}$. Note the results only depend on $|S|J$ so that taking $S_i = \pm 1$ instead of $S_i = \pm 3/2$ only corresponds to a redefinition of J .

Besides these usual terms of the double exchange model, we consider a hybridization $V_{i\eta k}$ connecting each site i of the nanostructure to some non-interacting environment η with eigenenergies $\epsilon_{\eta k}$ where k labels the different states in the respective environment, see Fig. 1. Such term allows one to describe, e.g., a surface or electrodes (leads) applied to the system for electric transport measurements. Altogether, this leads to the Hamiltonian

$$H = \sum_{ij\sigma} t_{ij} c_{i\sigma}^\dagger c_{j\sigma} - 2J \sum_i s_i S_i + \sum_{i\eta k\sigma} V_{i\eta k} c_{i\sigma} a_{\eta k\sigma}^\dagger + H.c. + \sum_{\eta k\sigma} \epsilon_{\eta k} a_{\eta k\sigma}^\dagger a_{\eta k\sigma}. \quad (2)$$

Send offprint requests to:

^a Present address: held@ifp.tuwien.ac.at

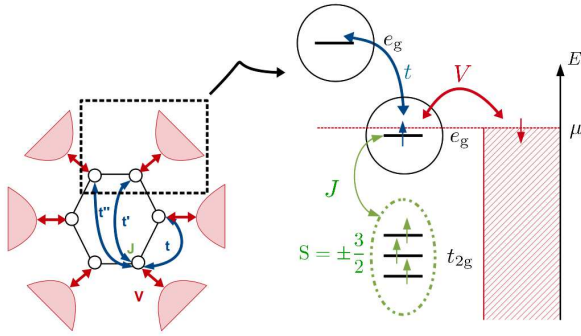


Fig. 1: Schematic representation of the model system consisting of six sites, each of them is connected to a lead via the hybridization strength $V_{i\eta k} = V\delta_{i\eta}$, and electrons can hop between the sites i and j of the nanostructure via hopping channels t_{ij} . Itinerant electrons interact with localized spins S at each site via Hund's coupling J .

In analogy to Refs. [5] we consider a nanoscopic system made of six-sites arranged in a ring structure. For the sake of simplicity, we will restrict ourselves to a configuration in which all sites are equivalent and each site is connected to its own paramagnetic metallic lead, i.e., $V_{i\eta k} = V\delta_{i\eta}$, and take a constant density of states $\rho = 1/(2D)$ for the non-interacting bath, where D is the bath half-bandwidth. As we will see, the competition between kinetic energy, hybridization, and Hund's exchange exhibits some very interesting properties, and can lead, depending on the parameters, to ferromagnetic (FM) or antiferromagnetic (AF) (and of course paramagnetic) short-range ordering of the localized spins.

In this paper, we solve the model (2) exactly on a six-site ring, and take it as a benchmark for testing the validity of a dynamical mean field theory (DMFT) [6] approximation. Let us note that the DMFT solution for the Kondo lattice model in the bulk was derived before by Furukawa [7]. In order to apply DMFT to a finite system, we employ its recently introduced nanoscopic version [5], which has been shown to be suitable to deal with complex nanostructures. The outline of the paper is as follows: In Sec. 2 we present the path integral method for the exact solution, and the DMFT scheme. In Sec. 2.1 we present the results obtained solving the model exactly, and we use them as a benchmark for DMFT in Sec. 2.2. Finally, we summarize our results in Sec. 3.

2 Method

Let us start with some simple symmetry considerations. In a six-sites system, with two possible alignments for each localized spin S_i , there are $2^6 = 64$ different possible configurations $\{S_i\}$. Since in the (high temperature) paramagnetic phase the Z_2 rotational symmetry is conserved, the overall alignment of the spins does not matter, thereby reducing the number of inequivalent configurations by a factor of two. In the following, 0 and 1 will represent the two different orientations of the localized spins. So, e.g., a configuration with only one spin-up would be represented by $\{100000\}$, which, in the paramagnetic phase, is also equivalent to $\{011111\}$.

In order to check the role of the connectivity, in the following we will consider similar cases as in Ref. [5]: (i) hopping is only possible to next neighbors ("NN t ") in which the number of inequivalent spin configuration is further reduced to eight, by symmetry, and (ii) hopping is equally possible to all sites ("all t "), with only four inequivalent spin configurations. The latter hopping topology is not a realistic one, as the hopping amplitude is a decreasing function of the inter-site distance. However it will be useful to study, in the philosophy of Ref. [5], the effect of enhanced connectivity without changing the geometry of the nanostructure. All these symmetry considerations are summarized in Table 1.

For an isolated nanostructure, i.e., without hybridization to the leads, the double exchange model can be solved exactly by calculating all eigenvalues and eigenstates of the Hamiltonian (2). This procedure becomes however computationally unfeasible if the number of sites of the nanostructure is very large, or if non-interacting leads are included, as it would require many additional bath-sites for an accurate description of the leads. We therefore employ a Green's function technique, were the non-interacting degrees of freedom can be integrated out exactly. In the Grassmann path-integral formulation [8] the expectation value of an observable \mathcal{O} is calculated as

$$\langle \mathcal{O} \rangle = \frac{1}{Z} \sum_{\{S_i\}} \int \mathcal{O} e^{-S\{S_i\}}, \quad (3)$$

where $Z = \sum_{\{S_i\}} \int e^{-S\{S_i\}}$ denotes the partition function of the system and the integration symbol $\int \equiv \prod_{i\sigma} \int \mathcal{D}[c_{i\sigma}^\dagger, c_{i\sigma}] \prod_{\eta k\sigma} \int \mathcal{D}[a_{\eta k\sigma}^\dagger, a_{\eta k\sigma}]$ represents the functional integral extending over the Grassmann variables $c_{i\sigma}^\dagger$ ($c_{i\sigma}$) and $a_{\eta k\sigma}^\dagger$ ($a_{\eta k\sigma}$) associated to the fermionic creation (annihilation) op-

configuration	NN t		all t	
	degeneracy	# of AF bonds	degeneracy	# of AF bonds
{000000}	2	0/6	2	0/15
{100000}	12	2/6	12	5/15
{110000}	12	2/6	30	8/15
{111000}	6	2/6	20	9/15
{101000}	12	4/6		
{100100}	6	4/6		
{101100}	12	4/6		
{101010}	2	6/6		

Table 1: Non-equivalent localized spin configurations for the six-site ring for both NN t and all t hopping topologies, taking into account Z_2 rotational symmetry and translational invariance.

erators. Finally, the action is given by

$$\begin{aligned} \mathcal{S}^{\{S_i\}} = & \int_0^\beta d\tau \left[\sum_{i\sigma} c_{i\sigma}^\dagger(\tau) (\partial_\tau - \mu) c_{i\sigma}(\tau) \right. \\ & + \sum_{i \neq j, \sigma} c_{i\sigma}^\dagger(\tau) t_{ij} c_{j\sigma}(\tau) - 2 \sum_i J s_i(\tau) S_i \\ & + \sum_{\eta k \sigma} a_{\eta k \sigma}^\dagger(\tau) (\partial_\tau + \epsilon_{\eta k} - \mu) a_{\eta k \sigma}(\tau) \\ & \left. + \sum_{i\eta k \sigma} V_{i\eta k} (c_{i\sigma}^\dagger(\tau) a_{\eta k \sigma}(\tau) + h.c.) \right], \quad (4) \end{aligned}$$

where $\tau \in [0, \beta)$ is the imaginary time, $\beta = 1/T$ is the inverse temperature, and μ is the equilibrium chemical potential. Hence the Green's function is defined as

$$G_{mn\sigma}(\tau) = \frac{1}{Z} \sum_{\{S_i\}} \int c_{m\sigma}(\tau) c_{n\sigma}^\dagger(0) e^{-\mathcal{S}^{\{S_i\}}}. \quad (5)$$

Since the non-interacting electron operators only enter quadratically in the action (4), we can integrate them out by a simple Gaussian integral [8], yielding the effective action

$$\begin{aligned} \mathcal{S}_{\text{eff}}^{\{S_i\}} = & \int_0^\beta d\tau \left[\sum_{i\sigma} c_{i\sigma}^\dagger(\tau) (\partial_\tau - \mu) c_{i\sigma}(\tau) \right. \\ & \left. + \sum_{ij\sigma} c_{i\sigma}^\dagger(\tau) t_{ij} c_{j\sigma}(\tau) - 2J \sum_i S_i s_i(\tau) \right] \\ & + \int_0^\beta d\tau \int_0^\beta d\tau' \sum_{ij\sigma} c_{i\sigma}^\dagger(\tau) \Delta_{ij}(\tau - \tau') c_{j\sigma}(\tau'). \end{aligned} \quad (6)$$

Here the hybridization function $\Delta_{ij}(\tau)$ takes into account the virtual processes of itinerant electrons hopping back and forth between the leads and the nanostructure. Its Fourier transform, analytically continued to the real axis, corresponds to the retarded function

$$\Delta_{ij}(\omega) = \sum_{\eta k} \frac{V_{i\eta k} V_{j\eta k}^*}{\omega + i\delta - \epsilon_{\eta k}}. \quad (7)$$

At this point it is convenient to recast the Green's function of the nanostructure (5) in terms of the effective action (6) considering the contribution of each configuration $\{S_i\}$ of the localized spins explicitly

$$G_{mn\sigma}(\tau) = \sum_{\{S_i\}} P^{\{S_i\}} G_{mn\sigma}^{\{S_i\}}(\tau), \quad (8)$$

via a functional integral for each configuration $\{S_i\}$

$$G_{mn\sigma}^{\{S_i\}}(\tau) = \frac{1}{Z^{\{S_i\}}} \int c_{m\sigma}(\tau) c_{n\sigma}^\dagger(0) e^{-\mathcal{S}_{\text{eff}}^{\{S_i\}}} \quad (9)$$

where we now only integrate the interacting degrees of freedom, i.e., $\int \equiv \prod_{i\sigma} \int \mathcal{D}[c_{i\sigma}^\dagger, c_{i\sigma}]$. The weights of the configuration-dependent Green's functions in Eq. (8) are defined by

$$P^{\{S_i\}} = \frac{Z^{\{S_i\}}}{\sum_{\{S_i\}} Z^{\{S_i\}}}, \quad (10)$$

where

$$Z = \sum_{\{S_i\}} Z^{\{S_i\}} = \sum_{\{S_i\}} \int e^{-\mathcal{S}_{\text{eff}}^{\{S_i\}}}. \quad (11)$$

The calculation of the probabilities Eq. (10) requires the evaluation of the determinant of $\mathcal{S}_{\text{eff}}^{\{S_i\}}$. This is more conveniently done in Fourier space where it takes the matrix form, in site indices i and j ,

$$\mathcal{S}_{ij\sigma}(\omega) = (-\omega - \mu + \Delta_{ij\sigma}(\omega) - J\sigma S_i) \delta_{ij} + t_{ij}. \quad (12)$$

Calculating these determinants (probabilities) as well as the Green's function for the inequivalent of the 2^6 spin configurations $\{S_i\}$ yields the exact summation of the Green's function of the nanocluster coupled to non-interacting leads.

Besides the exact solution, we have also employed DMFT. There are several versions of DMFT for treating nanoscopic or spatially inhomogeneous systems [5, 9, 10, 11] with minor differences. Here,

we perform our calculations in the same fashion as in Ref. [5], restricting ourselves to the 1-particle, i.e. DMFT, realization of the dynamical vertex approximation [12,13] applied to nanoscopic systems. The starting point of the DMFT scheme is the Green's function of the nanostructure, of which the generic matrix element of its inverse reads

$$\{G^{-1}\}_{ij\sigma}(\omega) = \omega\delta_{ij} - t_{ij} - \Delta_{ij\sigma}(\omega) - \Sigma_{ij\sigma}(\omega), \quad (13)$$

where Σ denotes the self-energy. For each of the (inequivalent) sites of the nanostructure, we define a local problem determining the associated Weiss field $\mathcal{G}_i^{0^{-1}} = [G_{ii}]^{-1} + \Sigma_{ii}$ out of the local block of site i of the Green's function G_{ii} , with an initial guess of the (local) self-energy Σ_{ii} (usually zero). This procedure maps each atom onto an effective one-body local problem where the local spin can either point up or down. Let us note that the DMFT approximation includes the local spins. That is, DMFT substitutes the actual localized spin configuration on the other sites by an effective Weiss field \mathcal{G}^0 , which in the paramagnetic phase is spin-independent. Hence localized spin up and down have the same probability and the interacting DMFT Green function of site i reads [7]

$$G_i(\omega) = \frac{1/2}{\mathcal{G}_i^{0^{-1}}(\omega) + J} + \frac{1/2}{\mathcal{G}_i^{0^{-1}}(\omega) - J}. \quad (14)$$

Since this has the form of a non-interacting Green's function averaged over a potential $\pm J$, Eq. (14) is temperature independent (which does not hold for DMFT Green's function in general). Mathematically this is equivalent to binary disorder. Hence, Eq. (14) allows us to determine a local self-energy $\Sigma_{ii} = \mathcal{G}_i^{0^{-1}} + G_i^{-1}$ for each site i . Using the calculated self-energies as an input for the Dyson equation (13) we can finally calculate a new Green's function for the nanostructure, and iterate the cycle self-consistently until convergence. [5] In the case we are considering all sites are equivalent due to the symmetry of the problem. Therefore we need to solve only one local problem, yielding a local self-energy which is the same for each site of the nanostructure.

2.1 Results: Exact Solution

In this section the exact results obtained are presented. As already mentioned, there are several competing energy scales in the problem. Therefore it is useful to describe the non-interacting ($J/t = 0$) and isolated ($V/t = 0$) "benzene" molecule first, and analyze separately the effects of the hybridization and of the interaction. The following analysis is summarized in the spectral function, connected to the retarded Green's function via the relation $A(\omega) = -\frac{1}{\pi}G_{ii}(\omega + i\delta)$, shown in Fig. 2.

When only the kinetic term of Hamiltonian (2) is taken into account, the nanostructure is translational invariant and the wavevectors $k = m\pi/3$ ($m = 0, \dots, 5$) are conserved quantum numbers. Setting the chemical potential $\mu=0$, yields the dispersion relation

$$E(k) = -2t \cos(k) - 2t' \cos(2k) - t'' \cos(3k), \quad (15)$$

where, t , t' , and t'' are the nearest neighbor, the next-nearest neighbor, and the next-next-nearest neighbor hopping amplitudes, respectively. In the following t sets our unit of energy, and the hopping configurations as defined by: (i) NN t case: $t' = t'' = 0$, and (ii) all t case: $t' = t'' = t$. The spectral function associated to this system is constituted by δ -like peaks corresponding to the six energy eigenstates (some of which are degenerate), and it is shown in the left panel of Fig. 2 for the NN t case (solid line). It is important to note that in both the NN t and all t case the spectral weight at the Fermi energy (E_F) is vanishing and the system is a band insulator.

In order to show what happens when the structure is connected to metallic leads, we restrict ourselves to the NN t case, but analogous considerations apply to any hopping topology. As already mentioned, the leads are bulk systems of non-interacting electrons described by a flat density of states $\rho = 1/(2D)$. We consider the broad-band limit $D \gg t$ (in order to avoid the particular physics arising at the edge of the leads' conduction band) and we set $D = 20t$ in the following. The most important effect of the hybridization between the ring and the non-interacting environment is the broadening of all peaks in the spectral function which are within the bandwidth of the leads, while the shift of the eigenenergies, i.e. the real part of the hybridization function, is $O(\omega/D)$. With increasing V , the discrete spectrum of the molecule evolves into a broad band (see Fig. 2, left panel).

The next step is to study what is the effect of the Hund's coupling J on such a nanoscopic system. In general, for a system of N sites, there are 2^N different configurations of the localized spins, which means that there are $2N2^N$ eigenstates. Most of them are degenerate in the non-interacting, paramagnetic system with translational invariance. In the presence of J and for a given configuration $\{S_i\}$, translational invariance is broken, and some of those degeneracies are lifted. At low enough temperatures, however, only the spin configurations corresponding to the lowest energy will be populated, so that the main effect of J is to increase the size of the gap. For large J , one can show that the size of the gap is $2J$ (see Fig. 2, middle panel). At higher temperature ($\beta t = 5$), due to the broadening of the Fermi-Dirac distribution, more states are occupied, and more energy eigenstates are visible in the spectral function (see Fig. 2, right panel).

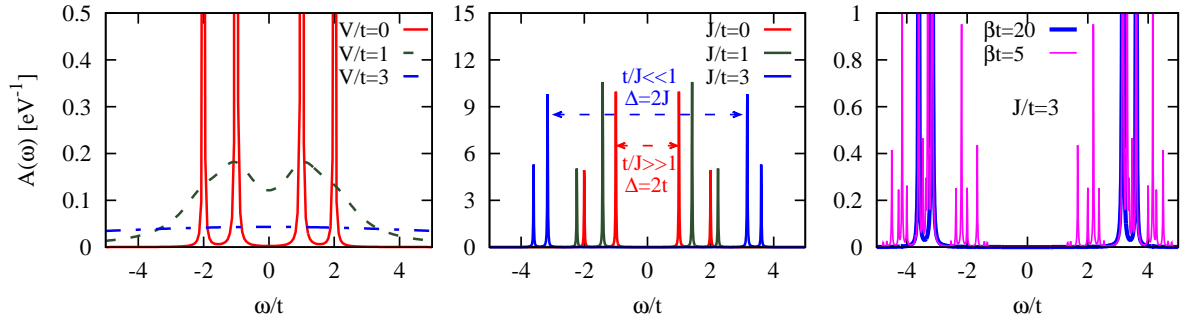


Fig. 2: Spectral function $A(\omega)$ for NN t in the broad-band limit $D = 20t$. Left panel: $J = 0$; the non-interacting levels are broadened either by the hybridization V or by a tiny cut-off $\delta/t = 0.01$. Middle panel: $V = 0$ for different values of J and $\beta t = 20$. One can clearly see that the gap Δ is controlled by t or J in the weak and strong coupling regimes, respectively. Right panel: Temperature dependence of the spectral function at $J = 3t$ and $V = 0$.

Moreover, due to the Hund's exchange that couples locally the itinerant and localized spins degrees of freedom, non-local (short-range) magnetic correlations arise between the localized spins, so that they mutually influence their orientation. We will see that, depending on the ratio between J and V , and on the density of the itinerant electrons, those correlations can favor a FM or AF alignment of the localized spins. The exact summation technique described in Sec. 2 allows us to calculate the probabilities $P[\{S_i\}]$ of Eq.(10), in order to show which spin configurations are energetically more favorable. As the probability of a configuration is -to a good approximation- only depending on the number of FM and AF bonds, regardless of the exact relative position of these bonds, we can identify four representative spin configurations, for each of the hopping topologies introduced above.

In the following we discuss general consideration in order to understand (or predict) what kind of magnetic correlation will affect the localized spins. In the isolated system (i.e. $V/t = 0$) only two energy scales are competing, namely the hopping t which tends to minimize the energy and delocalizes the itinerant electrons, and the Hund's coupling J , which couples their spins with the localized ones. Due to the Pauli principle, hopping processes between neighboring sites are only possible if the sites are occupied with one electron or two electrons with opposite spins. This leads to an effective AF correlation between the itinerant electrons, and an AF alignment is particularly favored at half-filling, when there is on average one electron per site. At the same time, in order to further minimize the energy, each localized spin tends to align to the spin of the itinerant electron (density) at the corresponding site. This mechanism leads to AF (superexchange) correlation between neighboring localized spins. On the other hand, when the

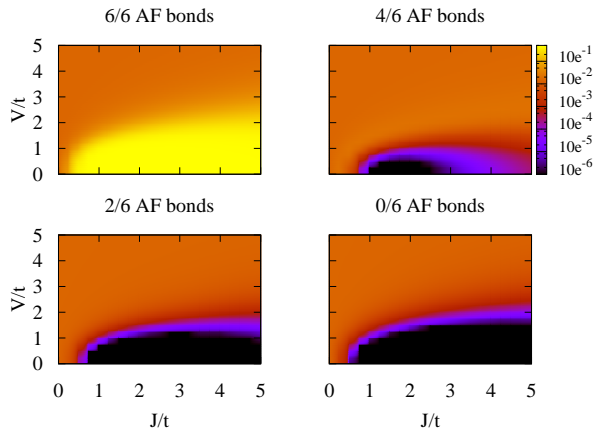


Fig. 3: Probability $P[\{S_i\}]$ for four representative configurations (out of 2^6) of localized spins, classified by the number of AF bonds, as a function of J and V , at $\beta t = 20$ and half-filling, in the NN t hopping topology. An AF kind of correlation of the localized spins is preferred for $J \gtrsim t$ and $J \gtrsim V$.

system is out of half-filling, the presence of empty (or doubly occupied) sites favors instead a FM double exchange correlation between localized spins. According to the considerations above, it is therefore interesting to study in detail the NN t case at non-integer density, e.g., quarter-filling, as well. The role of the hybridization is to effectively decouple the itinerant electron at each site from the other sites and the localized spin. The hybridization hence suppresses non-local magnetic correlations and leads to a more evenly distribution of spin configuration probabilities $P[\{S_i\}]$. In the following we analyze the probabilities of the different localized spins configurations as a function of V and

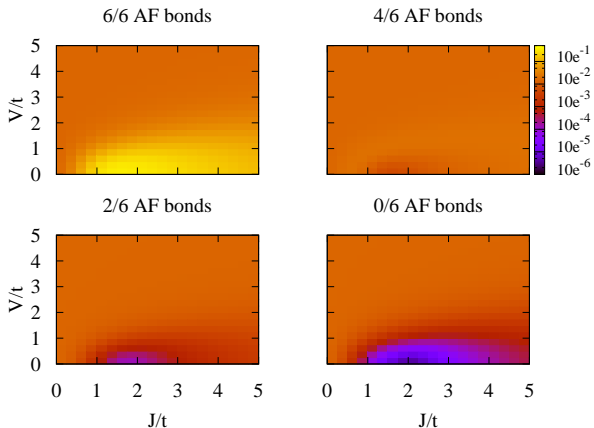


Fig. 4: As in Fig. 3 but at $\beta t = 5$. At high temperatures the system is characterized by more evenly distributed probabilities for the configurations of the localized spins.

J for NN t both at half- and quarter-filling. In Fig. 3 we show that for NN t at half-filling and $\beta t = 20$, an AF (short range) ordering of the localized spins is energetically favored in a region where $J \gtrsim V$, i.e. in the region where the probability of the configuration with six out of six bonds arranged AF is the highest (yellow region of the top left panel of Fig. 3). When the temperature is raised to $\beta t = 5$, states which are higher in energy become populated as well, leading to more evenly distributed probabilities, and therefore the AF correlation is weaker or confined to a smaller region of the $V - J$ plane, as shown in Fig. 4. However, one also expects that, independently of temperature, the probabilities of the different configurations to become evenly distributed even in the strong coupling limit $J \gg t$. This can be understood by considering that the short-range magnetic order arises due to the *interplay* of J and t . At $J \gg t$, the energy gain associated to hopping processes can be estimated in second order perturbation theory as $\Delta E \approx -t^2/2J$, and is vanishing for $J/t \rightarrow \infty$. As a consequence, the localized spins become uncorrelated in this limit and non-local correlations are suppressed.

In the quarter-filled case we find a similar behavior as for the half-filling, but, as expected, with dominant FM rather than AF configuration, i.e. the highest probability corresponds to the configuration with zero AF bonds (bottom right panel of Fig. 5). This result can be understood by considering that, at low densities, the itinerant electrons have an enhanced (with respect to half-filling) probability to hop to empty sites. These kind of processes are favored if the neighboring localized spins are aligned FM, and suppressed if they are aligned AF, since the process would cost an interaction energy of order $2J$. Recently the double exchange model

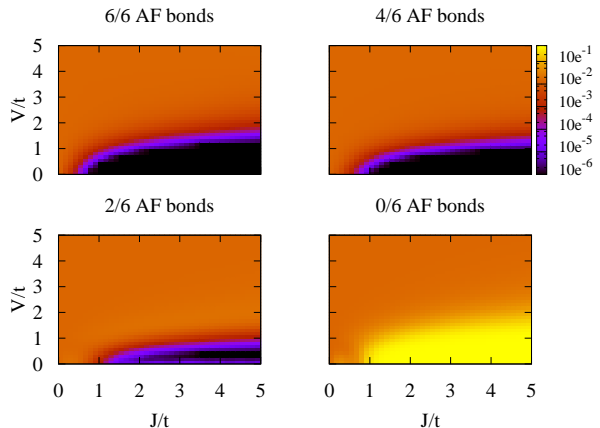


Fig. 5: Same as Fig. 3, but at quarter-filling, where FM (short range) ordering is favored when J becomes the dominating energy scale.

for a finite system for fully saturated t_{2g} spins has been analyzed in Ref. [14].

As we aim to compare the exact solution to DMFT, we also notice that DMFT has the property of becoming exact in the limit of infinite connectivity $z \rightarrow \infty$ [6]. One expects therefore that, increasing the connectivity of the system, non-local correlations to be averaged out and the mean field approximation to become reliable. As already mentioned, a possibility to do this, without changing the geometry of the nanostructure, is to introduce longer range hopping. It is therefore interesting to study how the system changes when we go from NN t to all t , i.e., increasing the connectivity from $z = 2$ to $z = 5$. In Fig. 6 we show that indeed the probabilities of the different spin configurations are in general more evenly distributed than for the NN t case, even at low temperatures, while AF short range order is still slightly favored in the strong coupling limit.

2.2 Comparison with DMFT

Let us turn to the DMFT solution, which for the specific case of the double exchange model is temperature independent (see Eq. (14)) and generally neglects non-local correlations. We hence expect DMFT to describe a system better if there is no (short-range) ordering of the spins, i.e., when the different spin configurations are rather equally important.

For the NN t system, the left panel of Fig. 7 shows that the spectral function of the exact solution exhibits many peaks at energies corresponding to the $N2^N$ eigenvalues of the Hamiltonian, while DMFT treats these states within mean field, and therefore predicts broad bands. Except for this

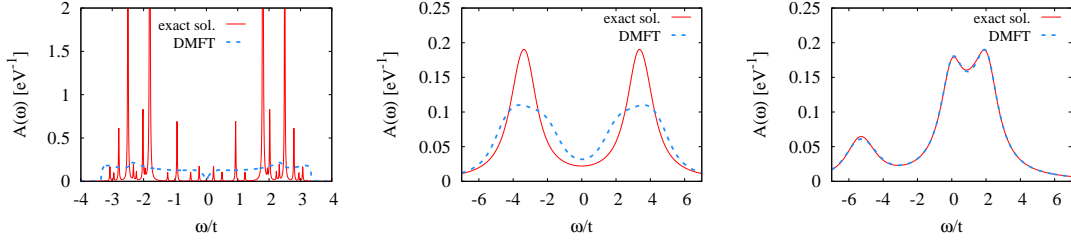


Fig. 7: Representative results of the comparison of the spectral function $A(\omega)$ between the exact solution and DMFT. Left panel: $J = 1.5t$, $V/t = 0$, and $\beta t = 5$ for NN t at half-filling which implies particle hole-symmetry for NN t . In the low-hybridization regime the exact solution displays many peaks which correspond to the eigenstates of the Hamiltonian, while DMFT rather predicts broad bands. Middle panel: $J = 3t$, $V = t$, and $\beta t = 20$ for NN t at half-filling; increasing the hybridization the DMFT description improves even at strong coupling. Right panel: $J = t$, $V = t$, and $\beta t = 20$ for all t ; increasing the connectivity the DMFT reproduces the exact solution, even in a non-perturbative regime. A similar behavior is observed also for quarter-filling (in the NN t topology) and in all other parameter regimes investigated.

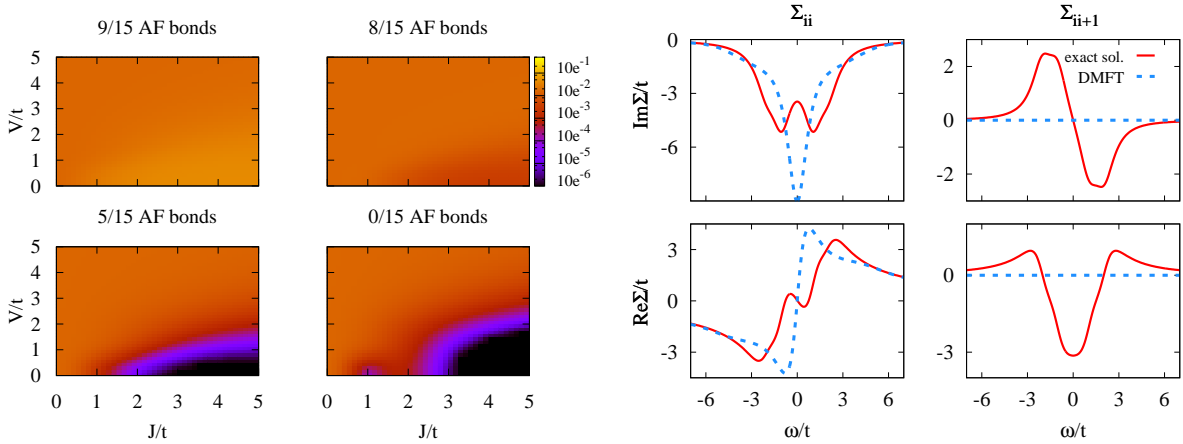


Fig. 6: Same as Fig. 3 but in the all t hopping topology. Increasing the connectivity of the system leads to much more evenly distributed probabilities.

Fig. 8: Local (Σ_{ii} , left panels) and non-local (for neighboring sites $\Sigma_{i,i+1}$, right panels) self-energy for $J = 3t$, $V = t$, $\beta t = 20$, and NN t hopping topology.

striking difference, the spectral function is qualitatively reproduced, and the DMFT spectrum is similar to a broadened version of the exact spectrum. In the presence of the hybridization V , the peaks get broadened anyhow. Hence, the finite- V spectrum predicted by DMFT is more similar to the exact one, as can be observed in the middle panel of Fig. 7. In the all t topology, where non-local correlations are washed away due to the high connectivity, the exact spectral function is almost exactly reproduced by DMFT, as shown in the right panel of Fig. 7.

A more precise characterization of the non-local spatial correlations between neighboring localized spins can be achieved considering the self-energies. In Fig. 8 and 9 we compare the exact and DMFT local (Σ_{ii}) and the non-local (between neighbor-

ing sites, $\Sigma_{i,i+1}$) self-energies corresponding to the spectral functions shown in the middle and right panel of Fig. 7, respectively.

In a Fermi liquid ground state, the local self-energy displays, around the Fermi energy E_F , a typical behavior $\Sigma_{ii}(0) \sim -\alpha\omega + i(\gamma + \delta\omega^2)$ with the coefficients $\alpha > 0$ and $\gamma, \delta < 0$. In the NN t case, shown in Fig. 8, the DMFT local self-energy is highly non-Fermi liquid, displaying a large maximum (in absolute value) in the imaginary part of Σ and a positive slope of the real part ($\alpha < 0$). These are the fingerprints of the depletion at E_F observed in the corresponding spectral function $A(\omega)$, which is also a consequence of the band gap that characterizes the non-interacting ring. Inter-

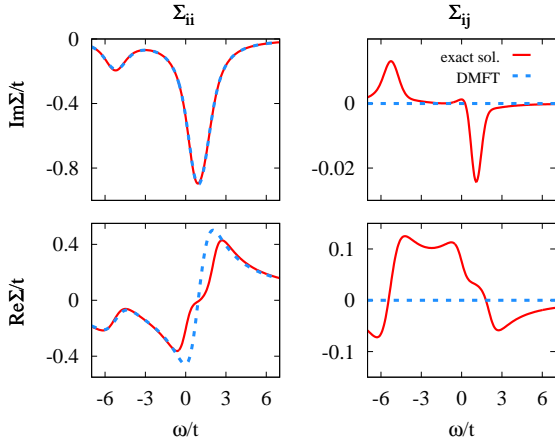


Fig. 9: Local (Σ_{ii} , left panels) and non-local (Σ_{ij} , equivalent for each pair $i \neq j$, right panels) elements of the self-energies for $J=t$, $V=t$, and $\beta t=20$, for both all t hopping topology.

estingly, the exact local self-energy behaves, in contrast, like in a Fermi liquid, and hence the comparison with DMFT looks poor. In absence of non-local correlations, the exact local self-energy would correspond to a scenario in which $A(\omega)$ would display a (renormalized) quasi-particle peak. The exact solution also predicts a pseudogap. However, this is generated by non-local magnetic fluctuations, e.g., by $\text{Re}\Sigma_{i,i+1}(0)$ between nearest neighbors (cf. also [12, 13, 15]). Non-local spatial correlations extend also to longer distances, and the corresponding elements of the self-energy (not shown) are quantitatively comparable to the nearest-neighbor one shown here.

In the all t case, shown in Fig. 9, the picture is qualitatively the same, with the fundamental difference, that the non-local contributions to the self-energy are sensibly smaller than the local ones, thus justifying that the DMFT spectral function well agrees with the exact one. Remarkably, due to the enhanced connectivity, the non-local self-energies remain small also at lower values of V/t , when the suppression of magnetic correlations due to the hybridization is less effective (not shown). This shows that for high enough connectivity, or strong hybridization, the Hund's coupling most likely does not result in a phase with short range order, and therefore can be treated reliably within a dynamical mean field approximation.

3 Conclusion and outlook

We have studied the double exchange model on a nanoscopic lattice. The advantage of this simple model is that it can be solved exactly also for finite

systems. This allows us to systematically study and understand the nature of approximations such as DMFT. Hence we can address the question: Where is this approximation sufficient, where does it fail quantitatively or qualitatively? We found DMFT to be reliable in a wide range of parameters. In particular we investigated the role of non-local correlations which are neglected in any DMFT-like calculation. These non-local magnetic correlations are suppressed if, e.g., the nano-cluster strongly hybridizes with metallic leads, or if it has a large coordination number, explaining the overall good quality of the DMFT predictions. After our analysis we can conclude that DMFT can be a suitable tool to study also more complex correlated nanostructures in this parameter range. However, if non-local correlations are not negligible, DMFT is not reliable anymore, and a better approximation is needed. In this respect, it is possible to extend the method in the spirit of DM^A [5, 12, 13, 16, 17, 18], which can account for those non-local correlations that are due to local fully irreducible two-particle vertices. This step is expected to improve the approximation significantly.

Acknowledgments

We would like to thank A. Toschi and G. Rohringer for useful discussions. We also acknowledge financial support from the Austrian Science Fund (FWF) through the Austria-Russia joint Project No. I610 (AV), I597 which is part of the DFG research unit FOR1346 (DR), and the Austrian Bundesministerium für Wissenschaft und Forschung and the European Union within the EU-Indian network MON-AMI (KH).

References

1. R. von Helmolt, J. Wecker, B. Holzappel, L. Schultz, and K. Samwer Phys. Rev. Lett. **71**, 2331 (1993); K. Chahara, T. Ohno, M. Kasai, and Y. Kozono, Appl. Phys. Lett. **63**, 1990 (1993); S. Jin, T. H. Tiefel, M. McCormack, R. A. Fastnacht, R. Ramesh, and L. H. Chen, Science **264**, 413 (1994); P. Schiffer, A. P. Ramirez, W. Bao, S-W. Cheong, Phys. Rev. Lett. **75**, 3336 (1995).
2. C. Zener, Phys. Rev. **82**, 403 (1951).
3. T. Sarkar, A. K. Raychaudhuri, and T. Chatterji, Appl. Phys. Lett. **92**, 123104 (2008); Appl. Phys. Lett. **92**, 123104 (2008); J. App. Phys. **101**, 124307 (2007); S. S. Rao *et. al.* App. Phys. Lett. **87**, 182503 (2005).
4. H. Das, G. Sangiovanni, A. Valli, K. Held, and T. Saha-Dasgupta, Phys. Rev. Lett. **107**, 197202 (2011).
5. A. Valli, G. Sangiovanni, O. Gunnarsson, A. Toschi, and K. Held, Phys. Rev. Lett. **104**, 246402 (2010); A. Valli, G. Sangiovanni, A. Toschi, and K. Held, Phys. Rev. B **86** 115418 (2012).

6. W. Metzner and D. Vollhardt, Phys. Rev. Lett. **62**, 324 (1989); A. Georges and G. Kotliar, Phys. Rev. B **45**, 6479 (1992); A. Georges, G. Kotliar, W. Krauth and M. Rozenberg, Rev. Mod. Phys. **68**, 13 (1996).
7. N. Furukawa, J. Phys. Soc. Jpn., **63**, 3214 (1994); N. Furukawa, *Physics of Manganites*, edited by T. A. Kaplan and S. D. Mahanti (Kluwer, New York, 1999).
8. W. Negele and H. Orland, *Quantum Many-Particle Systems* (Addison-Wesley, New York, 1987).
9. S. Florens, Phys. Rev. Lett. **99**, 046402 (2007).
10. M. Potthoff and W. Nolting, Phys. Rev. B **59**, 2549 (1999).
11. M. Snoek, I. Titvinidze, C. Tóke, K. Byczuk, and W. Hofstetter, New J. Phys. **10**, 093008 (2008).
12. A. Toschi, A. A. Katanin, and K. Held, Phys. Rev. B **75**, 045118 (2007); K. Held, A. A. Katanin, and A. Toschi, Prog. Theor. Phys. Supp. **176**, 117 (2008).
13. A. A. Katanin, A. Toschi, and K. Held, Phys. Rev. B **80**, 075104 (2009).
14. S. Henning, P. Herrmann, and W. Nolting, Phys. Rev. B **86**, 085101 (2012).
15. T. Maier, M. Jarrell, T. Pruschke, and M. H. Hettler, Rev. Mod. Phys., **77**, 1027 (2005).
16. H. Kusunose, J. Phys. Soc. Jpn. **75**, 054713 (2006).
17. C. Slezak, M. Jarrell, T. Maier, and J. Deisz, J. Phys.: Condens. Matter **21**, 435604 (2009).
18. The fully irreducible two-particle vertex has been recently calculated in G. Rohringer, A. Valli, and A. Toschi, Phys. Rev. B **86**, 125114 (2012).